Preprints, 15th IFAC Symposium on Control in Transportation Systems
June 6-8, 2018. Savona, Italy

Motorway Tidal Flow Lane Control

Konstantinos Ampountolas * **Henrique Salvaro Furtado** **
Rodrigo Castelan Carlson **

* *School of Engineering, University of Glasgow, Glasgow G12 8QQ, United Kingdom (e-mail: konstantinos.ampountolas@glasgow.ac.uk)*
** *Department of Automation and Systems, Federal University of Santa Catarina, Florianópolis – Santa Catarina 88040-900, Brazil (e-mail: henrique.salvaro@posgrad.ufsc.br; rodrigo.carlson@ufsc.br)*

Abstract: A traffic control case of particular importance occurs when inbound and outbound traffic on a motorway stretch is unbalanced throughout the day. This scenario may benefit of a lane management strategy called tidal flow (or reversible) lane control, in which case the direction of a contraflow buffer lane is reversed according to the needs of each direction. This paper proposes a simple and practical real-time strategy for efficient motorway tidal flow lane control. A switching policy based on the fundamental diagram, that requires only aggregated measurements of density (or occupancy), is adopted. A kinematic wave theory-based traffic flow analysis shows that the proposed strategy provides a Pareto-optimal solution. Simulation studies of the A38(M) Aston Expressway (Birmingham, UK), are used to demonstrate its operation. The results confirm an increase of motorway throughput and a smooth operation of the strategy.

Keywords: Tidal flow lane control; reversible lanes; fundamental diagram of motorway traffic

1. INTRODUCTION

Motorway network traffic management offers a number of control measures to alleviate traffic congestion, including ramp metering, variable speed limits, driver information and route guidance, mainstream control, and lane control (see, e.g., Papageorgiou et al. (2003)). Tidal flow lane control, a type of lane management (Obenberger, 2004), has received little attention in the literature. However, modern motorway networks include various infrastructure types and could support tidal flows to improve the infrastructure efficiency. The benefit of tidal flow (reversible lanes) operation is that the available capacity in each direction of traffic can be varied in response to highly directional inbound or outbound traffic flows. An odd number of lanes, usually three to seven, is required for effective tidal flow operation. The middle lane operates as a contraflow buffer zone to serve traffic in different directions. To ensure safe operation of contraflow, lane-use control signals with green arrows and red $\times$s located at overhead gantries are used wherever a particular movement is prohibited for designated lanes. A drawback, however, is the cost to efficiently control reversible lanes and the confusion to drivers and safety.

Worldwide the most common practice for tidal lane operation is manual or fixed-time control (Wolshon and Lambert, 2006; Wu et al., 2009). While in the first case it is particularly difficult for a human operator to evaluate the costs incurred by the transition period (Hausknecht et al., 2011), in the second case, typically, a static problem of lane reversal is solved (Khoo and Meng, 2008). These types of operation very often result in too early or too late reversal which have a negative effect on system performance (Glickman, 1973; Wu et al., 2009). A number of real-time tidal flow strategies have been proposed for urban arterials (Zhao et al., 2014), for motorways or uninterrupted facilities (Glickman, 1973; Zhou et al., 1993; Xue and Dong, 2000; Frejo et al., 2016), or both (Hausknecht et al., 2011). Except for Frejo et al. (2016) who proposed also a simple logic-based strategy, all proposed strategies are rather sophisticated or require advanced technologies.

Currently, many sites employ tidal flow operations including the A38(M) Aston Expressway (Birmingham, UK), A15 Canwick Road (Lincoln, UK), A61 London Road (Sheffield, UK), many wide boulevards and some freeways in Washington, D.C. (US), Coronado Bridge (San Diego, US), Tidal Busway (Eugene Oregon, US), a dozen of urban roads in Rio de Janeiro and São Paulo (Brazil), and a section of State Road SC-405 (Florianópolis, Brazil).

This paper develops a simple and practicable strategy for smooth and efficient tidal flow operations. The proposed policy is based on certain properties of the triangular Fundamental Diagram (FD) of motorway traffic and relies on real-time measurements of density or occupancy only. It is, thus, applicable in real-time to improve the bi-directional infrastructure efficiency. Section 2 introduces the motorway tidal flow lane control problem and presents the proposed FD-based policy. A theoretical analysis of the proposed strategy is presented in Section 3. Section 4 presents a microsimulation study of the application of the proposed approach to the A38(M) Aston Expressway (Birmingham, UK). Conclusions are given in Section 5.

2. MOTORWAY TIDAL FLOW LANE CONTROL

Consider a bi-directional motorway stretch with a contraflow buffer zone as shown in Fig. 1. The buffer lane is highlighted with red surfacing and literally permits tidal flow operations. The tidal (or reversible) lane switches direction at peak periods to provide extra capacity in one

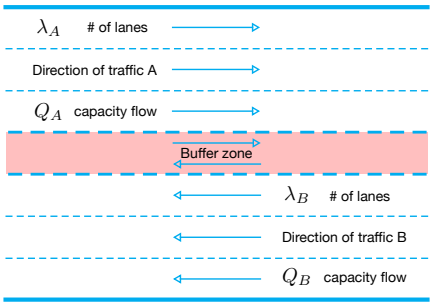

Fig. 1. A motorway stretch with a contraflow buffer zone.

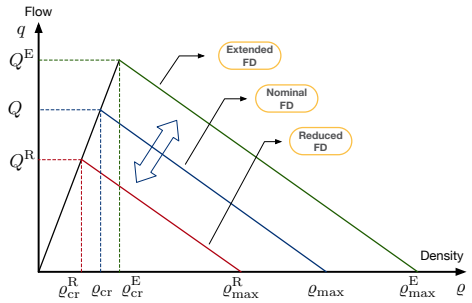

Fig. 2. Tidal flow operations described by the triangular FD.

direction (either A or B). Typically, this changes to four lanes in one direction and two lanes in the opposite direction maintaining the one lane buffer for safety reasons. In case of limited infrastructure (e.g., three lanes with one buffer lane) or motorway stretches with lane speed control, the buffer lane can be assigned to the direction of traffic with severe congestion without any other lane closure.

For analysis the most convenient is to assume that, under stationary traffic conditions, the bi-directional motorway stretch indicates a triangular nominal FD (nFD) as shown in Fig. 2. This theoretical model has the feature of being piecewise linear but not smooth. It has been proposed for the first time by Newell (Newell, 1993) as an alternative (simplified Kinematic Wave Theory) to solve the Lighthill-Whitham-Richard (LWR) model (Lighthill and Whitham, 1955; Richards, 1956), while it fits well with field empirical data as demonstrated in a number of practical studies. In the same vein, we define two other diagrams, namely reduced FD (rFD) and extended FD (eFD), to characterise tidal traffic flow operations. In particular under tidal flow lane control, the eFD characterises the traffic conditions in the direction of traffic with extra capacity, while the rFD characterises the opposite direction of traffic with reduced capacity. For simplicity, all FDs assume the same forward kinematic wave speed $w_{\mathrm{f}} = v_{\mathrm{f}}$, with v_{f} the free flow speed (the slope of the left branch of the FD), although different speeds can be assumed as appropriate. Schematically, the proposed control logic is illustrated with a bi-directional arrow in Fig. 2. It relies on the gentle switching of the nFD to the eFD or to the rFD under tidal flow lane control. It should be noted that all the FDs (nFD, rFD, eFD) can be readily estimated off-line provided experimental data. The following assumption guarantees smooth and efficient switching of the nFD to the eFD or to the rFD.

Assumption 1. If traffic conditions do not change rapidly with time, the stretches A and B should not simultaneously operate in the congested regime of the nFD.

For example, under stationary traffic conditions, both directions of traffic A, B in Fig. 1 will operate under the nFD with number of lanes $\lambda_A = \lambda_B = \lambda$ and maximum stationary flow $Q_A = Q_B = Q$. Now assume that the buffer lane switches direction to provide extra capacity in one direction of traffic, let's say to direction A (respectively, B). This results in the direction A (respectively, B) operating under the eFD while the direction B (respectively, A) operates under the rFD. Note that the efficient switching from the nFD to rFD requires the prevailing flow, q, of the free-flowing direction of traffic to satisfy $q \leq Q^R$, to avoid undesirable effects such as capacity drops.

The main idea behind the developed FD-based switching policy is to monitor in real-time the current prevailing densities ϱ_A and ϱ_B in both directions A, B, and compare them with the critical density ϱ_{cr} of the nFD and $\varrho^{\mathrm{R}}_{\mathrm{cr}}$ of the rFD (see Fig. 2). If one direction of traffic is heavily congested during peak hours (i.e., its critical density is higher than the critical density of the nFD) and the other direction of traffic free flows (i.e., its critical density is lower than the critical density of the rFD), then the buffer lane switches direction to provide extra capacity to the heavily congested direction of traffic; while the nominal capacity of the opposite direction is reduced to rFD. Switching is allowed if and only if both conditions are satisfied, otherwise (i.e., if both directions of traffic are congested or both uncongested) a do nothing policy is applied and both directions of traffic operate under the nFD with $\lambda_A = \lambda_B = \lambda$. The above control logic can be summarised in the following FD-based switching policy:

$$u(k) = \begin{cases} 1, & \text{if } \varrho_A(k) > \varrho_{\mathrm{cr}} \text{ and } \varrho_B(k) \leq \varrho^{\mathrm{R}}_{\mathrm{cr}}, \\ -1, & \text{if } \varrho_B(k) > \varrho_{\mathrm{cr}} \text{ and } \varrho_A(k) \leq \varrho^{\mathrm{R}}_{\mathrm{cr}}, \\ 0, & \text{otherwise}, \end{cases} \quad (1)$$

with $k = 1, 2, \ldots$ the discrete time index and $u(k)$ indicates the number of lanes opened or closed in each direction of traffic (see below for details). This control policy is executed in real-time every control period T. It should be noted that the control period T should be sufficient large to avoid oscillations (frequent switchings) and windup phenomena in dead zones where control does not affect the state of the system. Assumption 1 guarantees that the proposed scheme provides smooth and efficient tidal flow control operations. The basic steps of the FD-based tidal lane switching policy are given in Algorithm 1 (next page). Several points should be noted:

- The thresholds ϱ_{cr} and $\varrho^{\mathrm{R}}_{\mathrm{cr}}$ in (1) can be changed to $\varrho_{\mathrm{cr}} + \Delta$ and $\varrho^{\mathrm{R}}_{\mathrm{cr}} + \Delta^{\mathrm{R}}$ to compensate for possible uncertainties associated with the pre-specified critical densities, with Δ and Δ^{R} appropriate constants.
- Steps 2-4 and 6-8 of the algorithm ensure smooth tidal operations by allocating sufficient time for clearing the contraflow buffer lane and one lane from either A or B directions (to serve as a new buffer lane for safety).
- The FD-based policy can work with proxies of density, e.g., occupancies (available from inductive-loop detectors), without significant modifications of the main logic.
- The FD-based policy is robust because it does not rely on any forecasts (although forecasts of waiting queues in each direction of traffic can be incorporated into the logic). It relies only on the observable densities ϱ_A, ϱ_B and on the switching of the nFD to rFD or the eFD.

Algorithm 1: FD-based Switching Policy

Data: Critical densities $\varrho_{\rm cr}$, $\varrho_{\rm cr}^{\rm R}$ of nFD, rFD; number of lanes λ; control interval T.
Result: Control policy $u(k)$; $\lambda_A(k+1)$, $\lambda_B(k+1)$.
Initialise: Set $k \leftarrow 1$; $\lambda_A(k) \leftarrow \lambda$; $\lambda_B(k) \leftarrow \lambda$.;
begin
1 Enter new measurements $\varrho_A(k)$ and $\varrho_B(k)$ (over T);
if $\varrho_A(k) > \varrho_{\rm cr}$ ***and*** $\varrho_B(k) < \varrho_{\rm cr}^R$ **then**
2 Close access to buffer and B's current median lane;
3 Wait until both lanes are empty;
4 Open buffer lane for A's access;
5 Set $u(k) \leftarrow 1$;
else if $\varrho_B(k) > \varrho_{\rm cr}$ ***and*** $\varrho_A(k) < \varrho_{\rm cr}^{\rm R}$ **then**
6 Close access to buffer and A's current median lane;
7 Wait until both lanes are empty;
8 Open buffer lane for B's access;
9 Set $u(k) \leftarrow -1$;
else
10 Set $u(k) \leftarrow 0$; do nothing;
end
11 Set $\lambda_A(k+1) \leftarrow \lambda + u(k)$;
12 Set $\lambda_B(k+1) \leftarrow \lambda - u(k)$;
13 Set $k \leftarrow k+1$; go to step **1**;
end

The proposed FD-based policy (1) guarantees that both directions of traffic operate in the uncongested regime of either the nFD or rFD and eFD, which is characterised by a forward kinematic wave speed $w_{\rm f}$. As a special property of the triangular FD, free flow speed $v_{\rm f}$ applies to all uncongested conditions and thus $w_{\rm f} = v_{\rm f}$.

3. KINEMATIC WAVE THEORETICAL ANALYSIS

The following analysis, which is based on the Kinematic Wave Theory (KWT), provides a number of insights on the effectiveness of the proposed FD-based switching policy in terms of motorway capacity and throughput maximisation. Consider the closed (no on/off-ramps) bi-directional motorway stretch shown in Fig. 1 of length $\ell = \ell_A + \ell_B$ with a variable number of lanes in each direction of traffic, and different input demands; where ℓ_A and ℓ_B is the length of stretch A and B, respectively. Note that ℓ_A and ℓ_B are variable but bounded, given one buffer lane. Their length depends on the number of lanes assigned in each direction of traffic while ℓ is bounded by the existing infrastructure.

Let $\varrho_A(x)$ and $\varrho_B(y)$ be the density at location x and y, respectively. Let $F(\varrho_A(x), x)$ and $G(\varrho_B(y), y)$ be two location-dependent concave FDs that provide the outflow (throughput) at x and y when the local density is $\varrho_A(x)$ and $\varrho_B(y)$, respectively. Assume that the downstream infrastructure (off-ramps, exit-points, etc.) has enough capacity to discharge any desired outflows in both directions of traffic. Now assume that there is some directional flow disparity between the two directions of traffic and thus define as $f(x) = f(x, x+dx)/dx$ and $g(y) = g(y, y+dy)/dy$ the fraction of traffic exiting per unit length of road at x and y, respectively. Then, the prevailing bi-directional outflow in an interval $i_{x,y} = (x, y \mid x+dx; y+dy)$ is the sum of two products: (a) the product of the flow $F(\varrho_A(x), x)$ and the fraction of vehicles $f(x)dx$ exiting in $i_{x,0}$; (b) the product of the flow $G(\varrho_B(y), y)$ and the fraction of vehicles $g(y)dy$ exiting in $i_{0,y}$. The total bi-directional outflow is:

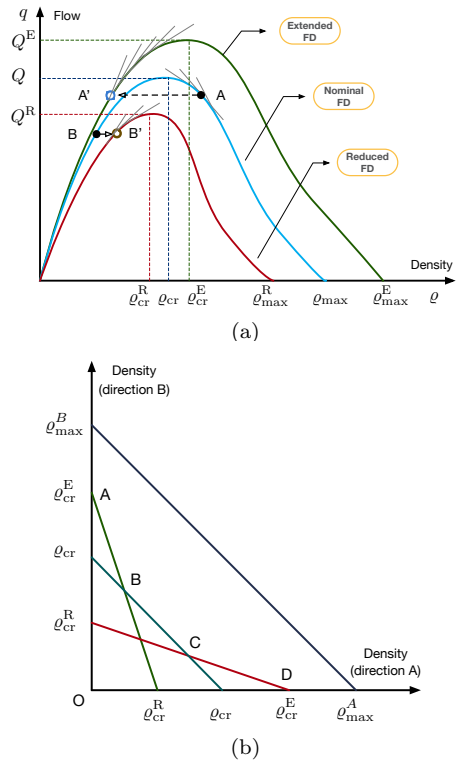

Fig. 3. (a) Tidal flow operation described by three generic fundamental diagrams; (b) Pareto efficient solutions in a (ϱ_A, ϱ_B) phase diagram. Region ABCD is the Pareto frontier.

$$O = \int_0^{\ell_A} F(\varrho_A(x), x) f(x)\, dx + \int_0^{\ell_B} G(\varrho_B(y), y) g(y)\, dy. \quad (2)$$

The total bi-directional accumulation of vehicles is

$$N = \int_0^{\ell_A} \varrho_A(x)\, dx + \int_0^{\ell_B} \varrho_B(y)\, dy. \quad (3)$$

The problem of bi-directional throughput maximisation now reads: maximise (2) subject to (3), where $\varrho_A(x)$ and $\varrho_B(y)$ are the variables to be optimised. This problem can be solved by introducing the Lagrangian associated with the constrained problem and then taking the appropriate partial derivatives equal to zero ($\varrho_A(x) > 0$, $\varrho_B(y) > 0$). From the first-order necessary conditions, it appears that the optimal solution $\varrho_A^*(x)$, $\varrho_B^*(y)$ must satisfy

$$f(x) w_A(\varrho_A^*(x), x) = g(y) w_B(\varrho_B^*(y), y) = \mu^*, \quad (4)$$

where μ^* is a Lagrange multiplier; and, $w_A(\varrho_A, x) \triangleq \partial F(\varrho_A, x)/\partial \varrho_A$ and $w_B(\varrho_B, y) \triangleq \partial G(\varrho_B, y)/\partial \varrho_B$ are the kinematic wave speeds of directions A and B, respectively.

First consider the case where F, G are unimodal nFD (see Fig. 3(a)) and the buffer lane is closed. The value of the Lagrange multiplier μ^* guarantees that the optimal distribution $(\varrho_A^*(x),\ \varrho_B^*(y))$ satisfies (3). Given that (3) is an equality constraint, μ^* can take any value in the real line, depending on N. If μ^* is positive, then w_A and w_B must be positive for all x and y, respectively. This suggests that ϱ_A and ϱ_B should be on the left branch of F and G for all x and y, respectively; i.e., both directions of traffic should be uncongested everywhere. Contrary, if μ^* is negative, then w_A, w_B must be negative and both directions of traffic should be congested everywhere.

Finally, if μ^* is zero, $|w_A| \approx 0$ and $|w_B| \approx 0$, i.e., both directions of traffic should be at flow capacity everywhere ($\varrho_A = \varrho_B \approx \varrho_{\text{cr}}$), while system's throughput is maximised.

Condition (4) also implies that the most popular direction of traffic (i.e., the one with the largest number of trips f or g) should have the smallest slope (w_A or w_B, respectively) in absolute value, i.e. the densities closest to critical and flows closest to capacity. Further, it suggests that the least popular direction of traffic with the smallest number of trips should have the largest positive slope, i.e., should be on the rising branch of the FD. This result also confirms the validity of Assumption 1, implying that if $f(x)$ is large for direction A (w_A should be small) then $g(y)$ should be sufficient small (and w_B should be sufficient large).

Consider now the case of instability, where flow disparity is significant between the two directions of traffic, congestion is developed in direction A while direction B free-flows as shown in Fig. 3(a) (e.g., traffic state A is on the congested regime while state B is on the uncongested regime of the nFD). In this case, the policy (1) opens the buffer lane for direction A and closes one lane in direction B ($u = 1$). This results direction A to operate under the eFD with number of lanes $\lambda_A = \lambda + 1$ while B operates under the rFD with number of lanes $\lambda_B = \lambda - 1$. This switching produces two waves as shown in Fig. 3(a), the right one (A,A$'$) is an accelerating rarefaction wave and the left one (B,B$'$) is a standing transition wave. The rarefaction wave forces congested state A in the nFD to meet state A$'$ in the uncongested regime of the eFD, where flow is maintained, speed is increased while density is substantially decreased to accommodate a largest number of trips. The standing wave, with speed virtually zero, forces state B in the nFD to meet state B$'$ in the uncongested regime of the rFD, where flow is maintained, speed is slightly decreased while density is slightly increased. As a special property of the triangular FD $w_A = w_B = w_f > 0$ and thus the switching waves (A,A$'$) and (B,B$'$) imply $f = g$ and $\mu^* > 0$, i.e., both directions of traffic should be uncongested everywhere and should be served with the same trip rate. The case $u = -1$ can be analysed using similar arguments.

In summary, the proposed tidal flow lane control and optimality condition (4) suggest that infrastructure and densities should be managed so as to maximise flow on the direction of motorway that contains the maximum number of desired destinations. Thus, it benefits both directions of traffic and is Pareto-optimal. Fig. 3(b) depicts the Pareto frontier of (1), i.e., the set of all Pareto efficient solutions for both directions of traffic under tidal lane control. Any hyperplane tangent to the Pareto frontier is a supporting hyperplane. Supporting hyperplanes are the three cases offered in (1). Maximisation of bi-directional exit flows is equivalent to the minimisation of the total time spent in the network, provided control independent inflows.

4. EMPIRICAL DATA AND SIMULATION RESULTS

4.1 Site and Empirical Data Analysis

The test site is the A38(M) Aston Expressway in Birmingham, which links the north of Birmingham City Centre to the M6 Motorway. The tidal flow stretch of the A38(M) is 1.1 mile long with seven lane carriageway. The central lane acts as a contraflow buffer lane as depicted in Fig. 4. An aerial view is provided in Fig. 5(a). During AM and PM peaks this typically changes to four lanes in one direction and two lanes in the opposite direction maintaining the one lane buffer. All seven lanes are managed with lane-use control signals with green arrows and red $\times$s located at overhead gantries as depicted in Figs 5(b) and 5(c). Typically, the southbound (SB) direction is congested during the morning commute peak and the northbound (NB) during the evening peak. Real flow-speed data from six lanes (one loop detector per lane) and spanning one month, were available for the calibration of the triangular FD (Fig. 2). The six detectors are located after the Gravelly interchange (Junction 6 of M6, Spaghetti Junction) towards A38(M). The real data were available from the Highways England "Motorway Incident Detection and Automatic Signals" (MIDAS) system in February 2016. The data were available in 15-min samples of flow (vehicles per 15 min) and speed (miles per 15 min). The empirical data were first used in an offline mode to calibrate the FD and to obtain its critical parameters for tidal flow control; then were used as reference for adjusting some simulation parameters.

Figs 6(a) and 6(b) depict empirical data for one month (February 2016) from one lane of both SB and NB directions of A38(M). Each measurement point on the FD corresponds to 15 min samples. Figs 6(a) and 6(b) confirm the existence of an FD for both SB and NB directions of A38(M) with moderate scatter on the congested regime. It can be seen that flow capacity for both directions is observed at a critical density $[40, 60]$ veh/mi, while free flow speed is around 50 mi/h. Lower flows are observed in the SB direction (compared to NB) due to merging of A38(M) with M6 at Junction 6.

Based on our analysis in Section 2, we employ the triangular FD (known as Newell's model), which fits well with empirical data. The flow–density relationship reads:

$$q = \begin{cases} v_{\text{f}}\, \varrho, & \text{if } \varrho \le \varrho_{\text{cr}} \\ q_{\text{cap}} \left(1 - \frac{\varrho - \varrho_{\text{cr}}}{\varrho_{\max} - \varrho_{\text{cr}}}\right), & \text{if } \varrho_{\text{cr}} < \varrho \le \varrho_{\max}, \end{cases} \tag{5}$$

with v_{f} the free-flow speed and $q_{\text{cap}} = Q$ the flow capacity. Figs 6(a) and 6(b) depict Newell's model (5) for $v_{\text{f}} = 45$ mi/h, $q_{\text{c}} = 2000$ veh/h/lane, $\varrho_{\text{cr}} = 45$ veh/mi/lane, and $\varrho_{\max} = 210$ veh/mi/lane.

4.2 Simulation Results

For testing the proposed control, the stretch of A38(M) was modelled in the microscopic simulator AIMSUN. Figs 6(c) and 6(d) show the obtained loop detector data from the simulator and Newell's model approximation for the NB and SB traffic, respectively. The model (5) is constructed with $v_{\text{f}} = 60$ mi/h, $q_{\text{cr}} = 2400$ veh/h/lane, $\varrho_{\text{cr}} = 40$ veh/mi/lane, and $\varrho_{\max} = 250$ veh/mi/lane. As can be seen, this calibrated model approximates well the Newell's model observed from the experimental data in Section 4.1 (cf. Figs 6(c) and 6(d) with Figs 6(a) and 6(b)). The simulation data were obtained from twelve replications with different seeds. Fig. 7(a) depicts the simulated demands at both ends of the motorway for a horizon of 250 min. These demand profiles were chosen so as to force the motorway going through all possible lane configurations under tidal lane control. The inflows and outflows at the

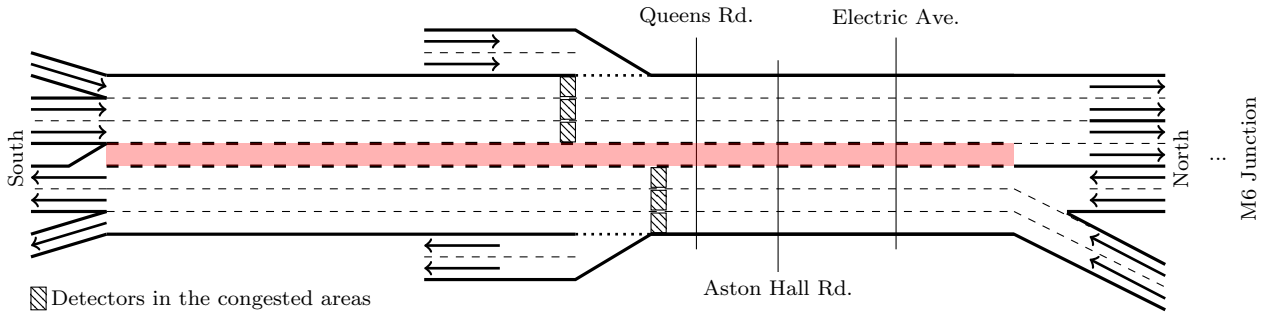

Fig. 4. Network topology of the simulated 1.1 mile tidal flow stretch of A38(M). The contraflow buffer zone is indicated with red colour.

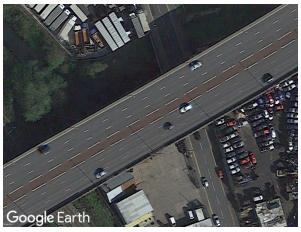

(a)

(b)

(c)

	Speed (mi/h)	Total Travel Time (veh×h)
No control	31.2 ± 1.9	828.3
With control	49.1 ± 4.9	427.7
Improvement	57.3%	48.4%

(d)

Fig. 5. (a) Top view of A38(M) at Electric Avenue; (b) gantry with SB view at around Aston Hall Road with two lanes SB, one buffer lane, and four lanes NB; and (c) gantry with NB view at around Electric Avenue with three lanes NB, one buffer lane, and three lanes SB. Map data ©2017 Google. (d) Quantitative measures obtained from the average of twelve replications.

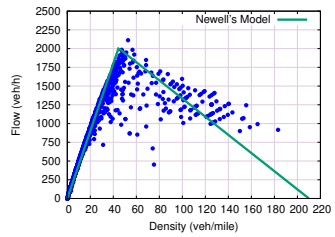

(a)

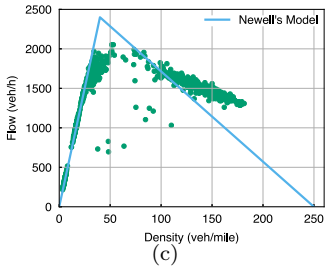

(c)

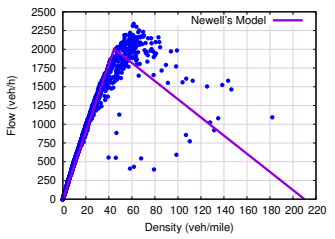

(b)

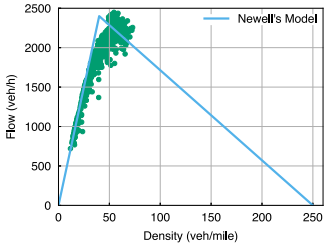

(d)

Fig. 6. (a) and (b): Loop detector data for one lane of SB and NB traffic, respectively, in February 2016 and approximated triangular FDs; (c) and (d): Simulation detector data for one lane of SB and NB traffic, respectively, and approximated FDs.

on-ramp and off-ramp near Queens Road were kept very low (see Fig. 4).

Based on the simulation data and FDs of Fig. 6(c) and 6(d), the control algorithm was applied with $\varrho_{\text{cr}} = \varrho_{\text{cr}}^{\text{R}} = 120$ veh/mi, $\Delta = 15$ veh/mi and $\Delta^{\text{R}} = -30$ veh/mi. Parameters Δ and Δ^{R} were determined via a trial-and-error procedure so as to achieve a satisfactory control behaviour. Aggregated data was collected for control at time intervals of $T = 10$ min, although an extensive analysis of an appropriate value was not carried out. After a decision for switching the lane configuration, a time window of one minute was provided for vehicles to exit the lane(s) to be closed for a given direction.

The simulation results obtained from twelve replications for each control case are shown in Fig. 5(d). Clearly, the proposed strategy provides significant improvements compared to the "no control" case where SB and NB directions operate with three lanes (and the contraflow buffer lane is closed). As can be seen under tidal flow lane control, the Total Time Spent (TTS) and space-mean speed are improved by 48% and 57%, respectively. These improvements underline the superiority of appropriate real-time tidal flow lane control and efficient use of the available infrastructure, which is underutilised in the no control case. Figs 7(c)–7(h) show the NB and SB flow, density, and speed at around the bottlenecks locations (see Fig. 4). The control action vertical lines indicate the switching time and the number of lanes for the control scenario in NB and SB direction after switching. The data corresponds to a replication with its results closest to the average values in Fig. 5(d).

The improved TTS stems from the increased throughput in the controlled scenario enabled by the proposed strategy, reflected by higher flows between around 140 to 180 minutes in the NB direction (Fig. 7(c)) and between around 10 to 70 minutes in the SB direction (Fig. 7(f)). Right at the beginning of the simulation, the high demand in the SB direction (Fig. 7(a)) causes a rapid increase in density, Fig. 7(g)). As consequence, the control strategy closes one lane in the NB direction and opens the buffer lane to the SB direction, as indicated in Fig. 7(b). The control strategy is able to bring the density back to the critical density ($\rho_{\text{cr}}^{\text{E}} = 160$ veh/mi), while in the no control scenario density remains at high values for the whole peak period. In the NB direction (Fig. 7(d)) a similar condition is observed, although higher values of density are reached by the controlled scenario due to the long control period ($T = 10$ min.). In both directions, the average speed is higher with control most of the time, but clearly during the peak-periods (Figs 7(e) and 7(h)). During the off-peaks

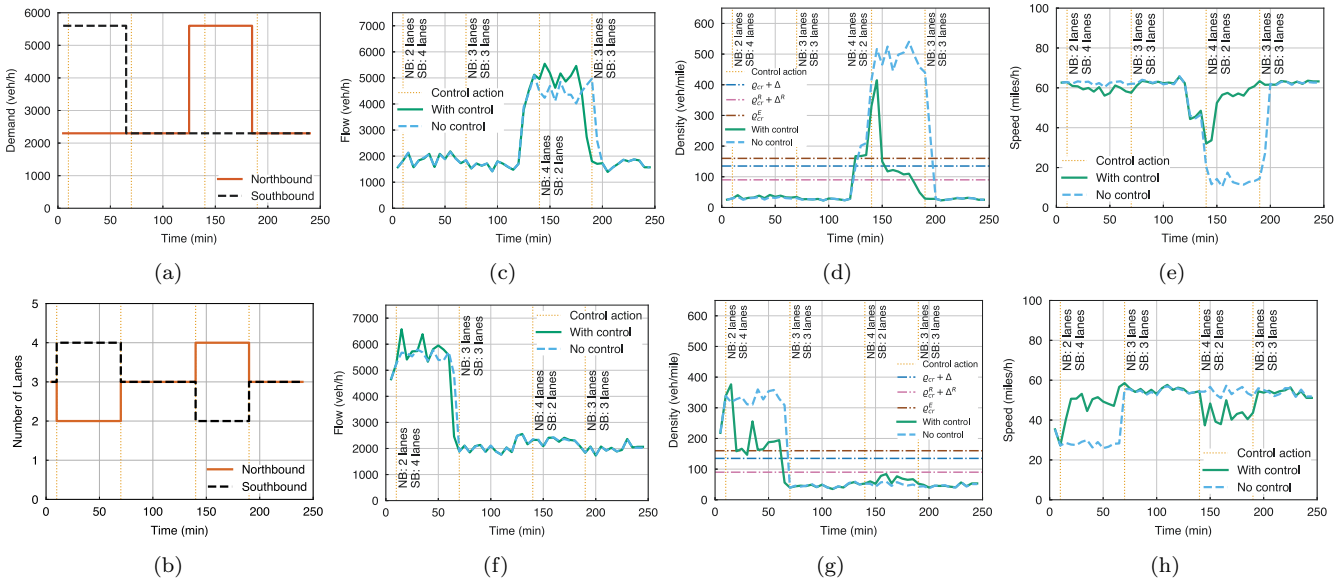

Fig. 7. Simulation results: (a) demand at the main entrances; (b) tidal lane control. Results with and without control; NB: (c) flow, (d) density, and (e) speed at around the bottleneck location. SB: (f) flow, (g) density, and (h) speed at around the bottleneck location.

a slight reduction in average speed, particularly in the SB direction, is observed. This is due to increased traffic friction due to the on-ramp (NB) or off-ramp (SB) whereas only two lanes are available in that direction.

5. CONCLUSIONS

This paper presented a practicable FD-based switching policy for smooth and efficient motorway tidal flow operations. The proposed policy relies on real-time observations of density or occupancy only and certain properties of the fundamental diagram of traffic. It does not rely on any forecasts nor real-time optimisation and thus it is applicable in real-time to improve the bi-directional infrastructure efficiency of motorway networks. Theoretical analysis based on the KWT has shown that the proposed policy leads (under certain conditions) to bi-directional motorway throughout maximisation. Remarkably, this policy provides Pareto efficient solutions for both directions of traffic under tidal flow lane control.

A microsimulation study of a site currently managing tidal flows, the A38(M) in Birmingham, UK, was used to demonstrate the operation of the proposed policy under realistic demand scenarios. Real experimental data from the A38(M) were used to calibrate the required fundamental diagrams. The simulation results confirmed an increase of motorway throughput and a smooth operation of the strategy. On-going work considers the calibration of the proposed policy and its comparison with other strategies for different infrastructures and realistic demand scenarios.

REFERENCES

Frejo, J.R.D., Papamichail, I., Papageorgiou, M., and Camacho, E.F. (2016). Macroscopic modeling and control of reversible lanes on freeways. *IEEE Transactions on Intelligent Transportation Systems*, 17(4), 948–959.

Glickman, T.S. (1973). Heuristic decision policies for the control of reversible traffic links. *Transportation Science*, 7(4), 362–376.

Hausknecht, M., Au, T.C., Stone, P., Fajardo, D., and Waller, T. (2011). Dynamic lane reversal in traffic management. In *14th International IEEE Conference on Intelligent Transportation Systems*, 1929–1934.

Khoo, H.L. and Meng, Q. (2008). Characterization and comparison of traffic flow on reversible roadways. *The IES Journal Part A*, 1(4), 291–300.

Lighthill, M.J. and Whitham, G.B. (1955). On kinematic waves II. A theory of traffic flow on long crowded roads. *Proceedings of the Royal Society of London A*, 229(1178), 317–345.

Newell, G.F. (1993). A simplified theory of kinematic waves in highway traffic Part I: General theory. *Transportation Research Part B*, 27, 281–287.

Obenberger, J. (2004). Managed lanes. *Public Roads*, 68(3), 48–55.

Papageorgiou, M., Diakaki, C., Dinopoulou, V., Kotsialos, A., and Wang, Y. (2003). Review of road traffic control strategies. *Proceedings of the IEEE*, 91(12), 2043–2067.

Richards, P.I. (1956). Shock waves on the highway. *Operations Research*, 4(1), 42–51.

Wolshon, B. and Lambert, L. (2006). Reversible lane systems: synthesis of practice. *Journal of Transportation Engineering*, 132(12), 933–944.

Wu, J.J., Sun, H.J., Gao, Z.Y., and Zhang, H.Z. (2009). Reversible lane-based traffic network optimization with an advanced traveler information system. *Engineering Optimization*, 41(1), 87–97.

Xue, D. and Dong, Z. (2000). An intelligent contraflow control method for real-time optimal traffic scheduling using artificial neural network, fuzzy pattern recognition, and optimization. *IEEE Transactions on Control Systems Technology*, 8(1), 183–191.

Zhao, J., Ma, W., Liu, Y., and Yang, X. (2014). Integrated design and operation of urban arterials with reversible lanes. *Transportmetrica B*, 2(2), 130–150.

Zhou, W.W., Livolsi, P., Miska, E., Zhang, H., Wu, J., and Yang, D. (1993). An intelligent traffic responsive contraflow lane control system. In *IEE Vehicle Navigation & Information Systems Conference*, 174–181.